JMEPEG (2022) 31:2909–2917
https://doi.org/10.1007/s11665-021-06455-z

1059-9495/$19.00

TECHNICAL ARTICLE

Corrosion Resistance Improvement of an Extruded Mg-Gd-Y-Zn-Zr-Ca via Aging Treatment

Xiang Yuan, Yuzhou Du, Dan Dong, Dongjie Liu, and Bailing Jiang

Submitted: 13 August 2021 / Revised: 19 October 2021 / Accepted: 5 November 2021 / Published online: 29 November 2021

The effects of aging treatment on corrosion properties of an extruded Mg-8.9Gd-2.8Y-1.8Zn-0.4Zr-0.2Ca (wt.%) alloy were investigated. The as-extruded alloy was consisted of un-dynamically recrystallized region containing lamellar long period stacking ordered (LPSO) phase and block-shaped LPSO phase, finely recrystallized grains and small amounts of Mg-RE phase. After aging treatment, part of lamellar LPSO phases was dissolved into the matrix and replaced by recrystallized grains. The size of recrystallized grain was increased from 1.8 μm for the as-extruded sample and to 3.5 μm for the peak-aged sample. Corrosion tests indicated that aging treatment effectively improved the corrosion resistance of the as-extruded Mg-8.9Gd-2.8Y-1.8Zn-0.4Zr-0.2Ca (wt.%) alloy. The lamellar LPSO phases with a low potential were preferentially corroded, and the homogeneous microstructure of the peak-aged sample effectively reduced the possibility of micro-galvanic corrosion. Hence, the peak-aged sample with a more homogeneous microstructure and small amount of lamellar LPSO phase showed a better corrosion resistance.

Keywords aging treatment, corrosion, LPSO, Mg-Gd-Y-Zn-Zr-Ca

1. Introduction

Nowadays, Magnesium alloys are widely used in aerospace, transportation and 3C fields because of their high specific strength, specific stiffness, and excellent damping performance (Ref 1-3). However, the low strength (Ref 4), poor ductility (Ref 5) and poor corrosion resistance (Ref 6) of Mg alloys compared with Al alloys restricted their application. Therefore, developing Mg alloys with good mechanical properties and superior corrosion resistance is the aim of researchers (Ref 7, 8).

It has been reported that Mg alloys containing long period stacking ordered (LPSO) phase exhibited high strength and ductility due to their unique strengthening and toughening effects of LPSO (Ref 5, 9). For example, small amount of Zn addition in Mg-3Gd-1.7Y-0.5Zr (wt.%) alloy resulted in the formation of LPSO phase, which gave rise the yield strength (YS) increasing by about 300% and elongation increasing by about 40% compared with the Mg-3Gd-1.7Y-0.5Zr alloy without LPSO phase (Ref 10). The corrosion properties of Mg alloys containing LPSO have also been widely researched (Ref 11, 12). However, there are contradictory conclusions about the effects of LPSO phase on corrosion properties of Mg alloys. It was reported that lamellar LPSO phase acting as a barrier protected Mg-substrates from being corroded (Ref 13). A Mg-Zn-Y-Al alloy containing LPSO phase with a good corrosion resistance was obtained (Ref 14). However, several investigations indicated that LPSO phase deteriorated the corrosion resistance of Mg alloys (Ref 15, 16). For instance, a Mg alloy containing lamellar 14H-LPSO exhibited an inferior corrosion resistance because of the LPSO phase acting as cathodic and accelerating corrosion rate (Ref 16).

Recently, Ca addition in Mg alloys attracted attentions because of its ability to improve aging hardening response of Mg alloys (Ref 17) by refining precipitates. For instance, a yield strength of 345 MPa and ultimate tensile strength of 405 MPa were obtained by extruding a Mg-7.5Gd-2.5Y-3.5Zn-0.9Ca-0.4Zr (wt.%) alloy (Ref 18); a Mg-5.1Zn-3.2Y-0.4Zr-0.4Ca (wt.%) alloy extruded at 350 °C exhibits a yield strength of 373 MPa and an ultimate tensile strength of 403 MPa (Ref 19). However, the corrosion properties of such series of Mg alloys have seldom been investigated. Therefore, a Mg-Gd-Y-Zn-Zr-Ca alloy was selected and the corrosion behavior before and after aging treatment were investigated in the objective to further elucidate the relationship between the microstructure and properties.

1.1 Experimental Procedures

High quality Mg-8.9Gd-2.8Y-1.8Zn-0.4Zr-0.2Ca (wt.%) ingot with a diameter of 92 mm were mainly fabricated by pure Mg ingot (99.95%), Gd (99.95%), Zn (99.95%), Mg-Y (wt.%) Mg-25Gd (wt.%) master alloys and Mg-30Zr (wt.%), under a mixed atmosphere of CO_2 and SF_6 with the ratio of 99:1. The detailed fabrication method could be referred to (Ref 20). Before hot extrusion deformation, the ingot was firstly homogenized at 430°C for 8h with water quenching above 80°C, the homogenized alloy and extrusion die were preheated at 420°C for 2h, then the extruded rod for experiment with a

Xiang Yuan and **Dan Dong**, School of Materials Science and Engineering, Xi'an University of Technology, Xi'an 710048, People's Republic of China; and **Yuzhou Du, Dongjie Liu,** and **Bailing Jiang**, School of Materials Science and Engineering, Xi'an University of Technology, Xi'an 710048, People's Republic of China; and Shaanxi Province Engineering Research Center for Magnesium Alloys, Xi'an University of Technology, Xi'an 710048, People's Republic of China. Contact e-mail: duyuzhou@xaut.edu.cn.

diameter of 49 mm was conducted at the temperature of 460°C with an extrusion ratio of 5:1 and an extrusion rate of 0.1mm/s. Part of the extruded samples were aged at 200°C for different times to obtained aging hardening curve.

The specimens for microstructural observation were cut along extrusion direction. The samples were firstly ground to 4000 grift using SiC papers and polished. Then, the samples were etched with 4% nitric acid alcohol. Microstructure were examined by a GX-71 optical microscope (OM) and a JSM-6700F scanning electron microscope (SEM) with an energy-dispersive spectrometer (EDS) at an operating voltage of 30 kV. The average grain size and phase volume fraction were calculated by Image-Pro Plus. X-ray diffraction (XRD) was carried out on an XRD-7000 using a Cu target with a scanning angle from 20° to 90° with a scanning speed of 4°/min.

Samples with dimension of 10 mm×10 mm×5 mm were mounted into epoxy resin with exposed surface area of 1 cm^2 to evaluate the hydrogen evolution testing in 3.5% NaCl solution at ambient temperature. The hydrogen volume was recorded during immersion for different times. The corrosion products were ultrasonically cleaned in 200 g/L CrO_3, 20 g/L Ba $(NO_3)_2$ and 10 g/L $AgNO_3$ solution. The weight loss was measured by a FA1004B analytic balance. The corrosion morphology was characterized by SEM.

The specimens for electrochemical tests were 15 × 15 mm. Electrochemical measurement was carried out in 3.5% NaCl solution with an exposed area of 1 cm^2. PARSTAT40000 Electrochemistry workstation was used for electrochemical measurements at ambient temperature. Electrochemical measurement was conducted by using a classical three electrode cell matched with the counter electrode of Pt, reference electrode of saturated calomel electrode (SCE) and the working electrode of sample surface itself. The potentiodynamic polarization was measured. Measurement regions were set from − 0.25 to 0.25 V vs. open circuit potential (OCP) at a constant scanning rate of 1 mV/s after an initial delay of 3600s. The electrochemical impedance spectroscopy (EIS) was performed with the scan frequency ranging from 10^5 Hz to 0.01 Hz and amplitude of 10 mV with respect to the OCP. The electrochemical tests were repeated at least three times to ensure the reproductivity, and then the obtained Nyquist and Bode curves fitted by using the ZSimDemo 3.30 software.

2. Results

2.1 Aging Response of the As-Extruded Alloy

Figure 1 shows the age-hardening curve of the as-extruded sample. The hardness of the as-extruded Mg-Gd-Y-Zn-Zr-Ca alloy was firstly increased and then decreased with increasing aging time. The as-extruded alloy with the hardness of 92 HV was increased to 98 HV after aging treatment for 24 h, indicating that the alloy exhibited a certain aging hardening response.

3. Microstructure

Figure 2 shows the optical micrographs of the as-extruded and peak-aged samples. Block-shaped phase, unDRXed region containing lamellar phase, finely recrystallized grain and

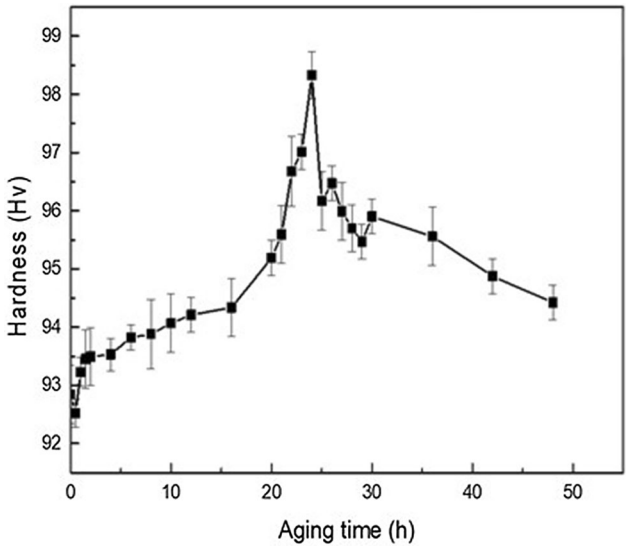

Fig. 1 Age-hardening curves of the as-extruded alloy

fragmented particles could be observed in the as-extruded and peak-aged samples. However, the fraction of phases in the as-extruded and peak-aged samples differed significantly. Studies has demonstrated that the block-shaped and lamellar phases were LPSO phases (Ref 9, 21). In addition, the volume faction of lamellar LPSO phase was decreased from 7.4 to 2.3% after aging treatment, while the volume fraction of block-shaped LPSO phase changed little. Therefore, it could be inferred that part of the LPSO phase dissolved into the matrix during aging treatment. Furthermore, the as-extruded alloy contained about 5.7 vol.% unDRXed regions, while the peak-aged sample exhibited a completed recrystallized microstructure. The average recrystallized grains size of the peak-aged sample was about 3.5 μm.

Figure 3 shows the SEM images and XRD patterns of the as-extruded and peak-aged samples. Small granular phase distributed in the vicinity of block-shaped LPSO phase in the two samples. From the enlarged image (Fig. 3b), numerous amounts of lamellar phases with various orientations existed in the DRXed grains of the as-extruded sample (Fig. 3b). Additionally, the dynamically recrystallized grains mainly distributed around the block-shaped LPSO phase for the as-extruded sample. However, the recrystallization region existed not only at the block-shaped LPSO phase but also at the region far from the second phases after aging treatment. It indicated that recrystallization occurred during aging treatment, which was observed in the as-forged Mg-6Gd-2Y-1Zn-0.3Zr and extruded Mg-8.2Gd-3.8Y-1Zn-0.4Zr alloys (Ref 15, 22). It has been reported that the block-shaped LPSO phase was hardly to be plastically deformed during extrusion process, which resulted in the pile-ups of dislocation between Mg matrix and block-shaped LPSO phase (Ref 23). Consequently, dynamic recrystallization was detected in these regions for the as-extruded sample. Additionally, particle stimulated nucleation (PSN) of LPSO phase was another factor of recrystallization (Ref 23, 24). Since the recrystallization was a process to release stress in local region (Ref 25), and the gradient dislocation existed at the interface, the recrystallized grain growth was considered to be stimulated preferentially at the location with high dislocation density and then gradually expand to the position with low dislocation density (Ref 26).

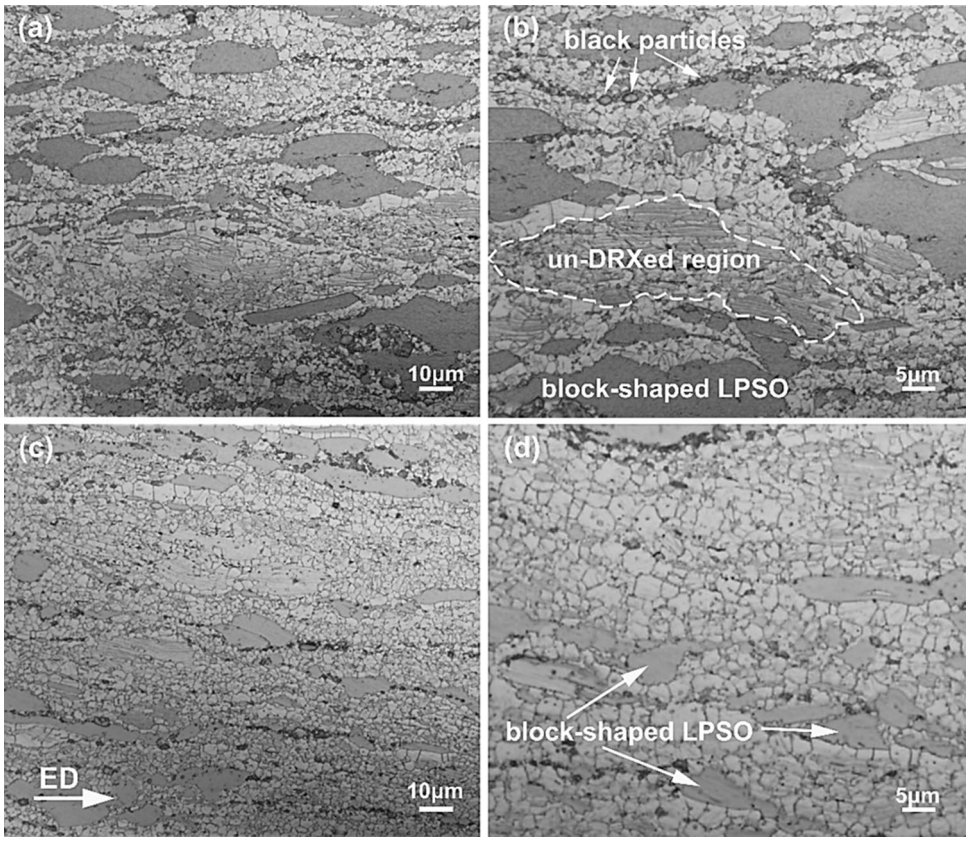

Fig. 2 Optical images of the (a, b) as-extruded and (c, d) peak-aged samples

It was noteworthy that the recrystallization accompanied by dissolution of lamellar LPSO dissolved during aging treatment, which could be found from both OM and SEM results. It has confirmed that lamellar LPSO phase are less thermostable than block-shaped LPSO in interdendritic region (Ref 27). Aging treatment accelerated the diffusion rate and increased the solid solubility of Gd and Y in Mg. Additionally, the lamellar LPSO phase distributed within the recrystallized grains, thus the solute atoms of the LPSO phase can directly diffused into the recrystallized grains. This was beneficial for the dissolution of lamellar LPSO phase. The dissolution of LPSO into Mg alloy during recrystallization has been reported in Mg-4.3Gd-3.2Y-1.2Zn-0.5Zr (wt.%), Mg-6Gd-2Y-1Zn-0.3Zr (wt.%) and Mg-8.2Gd-3.8Y-1.0Zn-0.4Zr (wt.%) alloy (Ref 15, 27, 28).

The EDS results of the as-extruded and peak-aged sample in Fig. 3 are presented in Table 1. The block-shaped LPSO phase marked A and C in the as-extruded and peak-aged alloys contained Mg, Y and Zn. The bright granular phase marked B in the as-extruded sample were found to contain a large amount of Gd and Y. In order to further confirm the phases in the two samples, XRD was conducted, which is shown in Fig. 3(e). It could be seen that no obvious difference was detected for the two samples. The main phases of the as-extruded and peak-aged samples were α-Mg, LPSO phase and Mg_5(Gd, Y). It has been confirmed the existence of Mg_5(Gd, Y) in Mg-13Gd-4Y-2Zn-0.5Zr (wt.%) and Mg-9Gd-4Y-2Zn-0.5Zr (wt.%) alloy (Ref 29, 30). Therefore, it is inferred that the as-extruded and peak-aged Mg-Gd-Y-Zn-Zr-Ca alloy contained lamellar LPSO phase, block-shaped LPSO phase, Mg_5(Gd, Y) and Mg matrix.

4. Corrosion Properties

4.1 Immersion Tests

Figure 4(a) demonstrates the hydrogen evolution of the two samples immersed in 3.5% NaCl solution. The as-extruded sample exhibited a much higher hydrogen evolution compared with the peak-aged sample, indicating that aging treatment effectively improved the corrosion resistance of Mg-Gd-Y-Zn-Zr-Ca alloy. Figure 4(b) presents the weight loss of the samples after immersion for 24, 48 and 100 h. The peak-aged sample exhibited an obvious lower weight loss compared with the as-extruded sample. With the immersion process was carried out for 24 h, the corrosion morphology of the as-extruded and peak-aged samples were given in Fig. 4(c). It could be clearly seen that the corrosion area and depth of the as-extruded sample were much more severe than the peak-aged sample, which was consistent with the hydrogen evolution and weight loss results.

4.2 Electrochemical Measurements

To further investigate the corrosion properties of the as-extruded and peak-aged samples, potentiodynamic polarization test and electrochemical impedance spectroscopy (EIS) of the two alloys were measured through immersing in 3.5% NaCl solution at ambient temperature, which were shown in Fig. 5. Generally speaking, corrosion potential (φ_{corr}) in potentiodynamic polarization curves represented the corrosion tendency, which reflected corrosion possibility from the viewpoint of thermodynamic. However, corrosion current density (I_{corr}) represented corrosion rate, which reflected the kinetics during

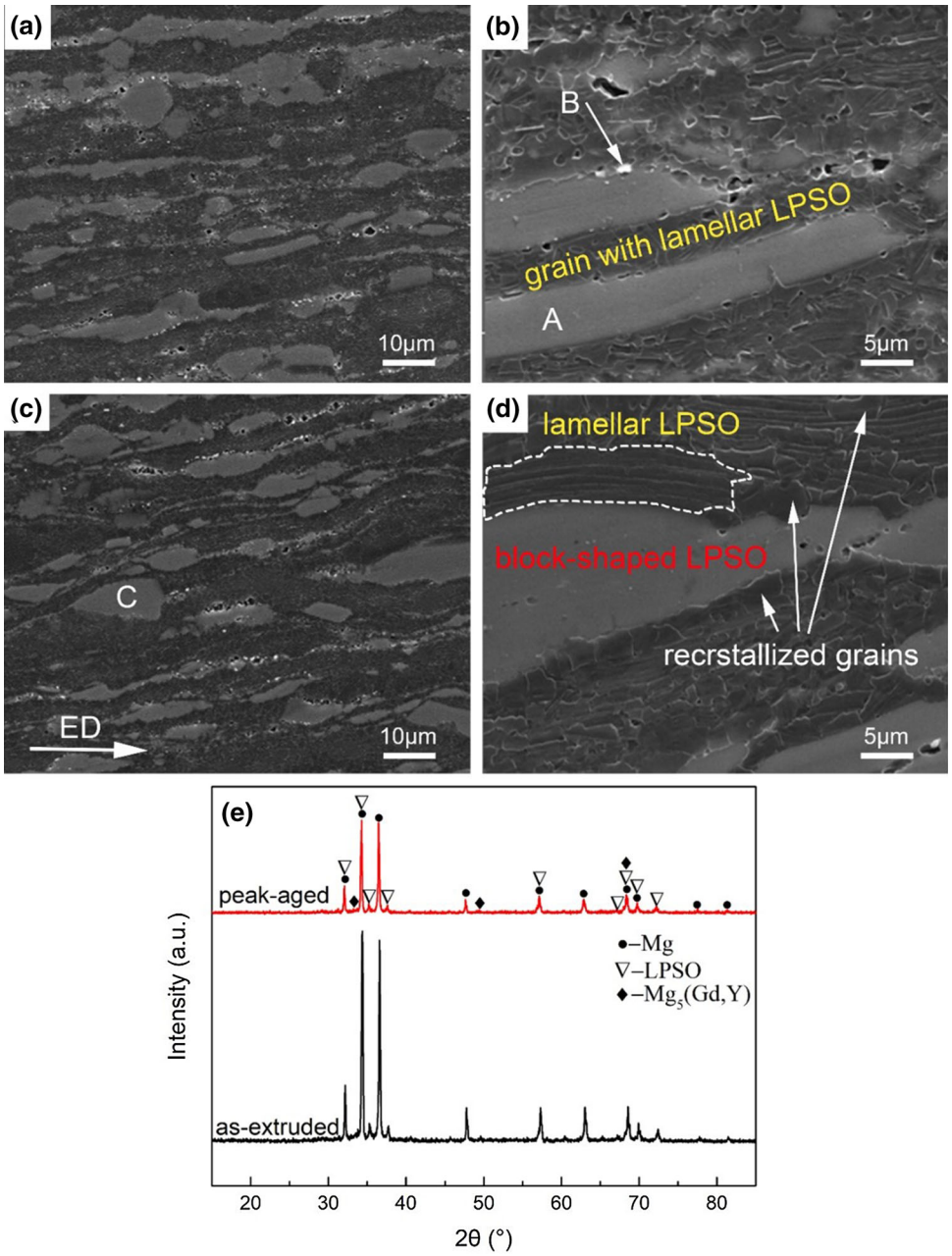

Fig. 3 SEM images of the (a, b) as-extruded and (c, d) peak-aged samples; (e) XRD patterns of the two samples

Table 1 EDS results of the as-extruded and peak-aged samples

Sample	Position	Atomic%			
		Mg	Gd	Y	Zn
As-extruded sample	A	91.21	3.2	1.68	3.91
	B	70.63	12.11	17.26	–
Peak-aged sample	C	89.63	3.75	1.91	4.71

corrosion process. In the anode branch of the polarization curve in Fig. 5(a), when I_{corr} was constant, φ_{corr} of the peak-aged alloy was higher than that of the as-extruded sample, indicating that corrosion was more likely to occur in the as-extruded alloy. When the φ_{corr} was constant, the peak-aged alloy exhibited a smaller I_{corr} value compared with the as-extruded sample, indicating that the corrosion rate was significantly lower than the sample in the extruded state. Therefore, the as-extruded alloy was more easily corroded than peak-aged alloy. From the value of φ_{corr} and I_{corr} summarized in Table 2, φ_{corr} increased from − 1.63 to − 1.52 V after aging treatment. The shift to positive direction of corrosion potential was resulted from the reduction of LPSO phase with a lower potential after aging treatment according to mixed-potential theory (Ref 31). In addition, the I_{corr} of the as-extruded alloy was about 3 times higher than that of the peak-aged alloy. The peak-aged sample exhibited a much less LPSO phase, which would reduce the formation of micro-galvanic corrosion. Consequently, the I_{corr} was significantly decreased. High I_{corr} and low φ_{corr} value

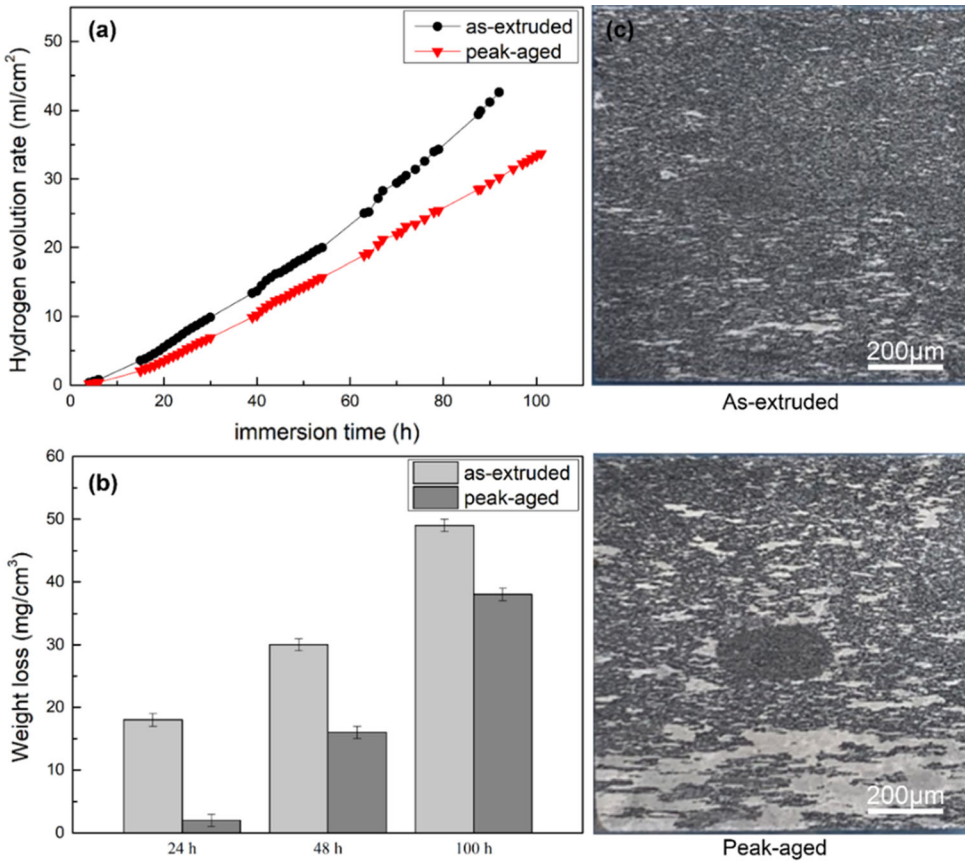

Fig. 4 (a) Hydrogen evolution curves, (b) weight loss of samples immersed in 3.5 NaCl%, (c) corrosion morphology of samples immersed in 3.5% NaCl for 24 h

indicated that the corrosion resistance of the as-extruded alloy was inferior to the peak-aged alloy.

The EIS spectra of the as-extruded and peak-aged samples are presented in Fig. 5(b), (c) and (d). The capacitive in high frequency region was associated with electric double layer at the surface between matrix and NaCl solution, while the medium frequency capacitive loop was related to the density of the corrosion layer on sample surface (Ref 32). The as-extruded and peak-aged alloys displayed two capacitive loop but different radius of loop (Fig. 5b), which indicated that corrosion resistance differed for the two samples, but corrosion mechanism was similar (Ref 33). In addition, the radius value of capacitive loop of the peak-aged alloy was larger compared with that of the as-extruded alloy, indicating that the peak-aged sample had a higher charge transfer resistance.

The fitting equivalent circuits of EIS spectra are given Fig. 5(e), (f), and the corresponding parameters are listed in Table 2, where *Rs* was the solution resistance with a relative constant value, indicating that the immersion conditions were practically invariant (Ref 15); R_f was the resistance of the corrosion products and R_{ct} was the charge transfer resistance. The fitting results in Table 2 showed a lager R_{ct} value for peak-aged alloy, indicating a higher charge transfer resistance and a lower dissolution rate of matrix (Ref 34), which was a result of reduction of micro-galvanic corrosion after aging treatment. A higher R_f value of peak-aged alloy indicating that the corrosion product of the peak-aged alloy was more stable. This was because the increase of recrystallized grains and more homogeneous microstructure after aging treatment which beneficial for the formation of Mg $(OH)_2$ passivation film (Ref 33). The constant phase element (CPE) resembles a capacitor, which was used to explain the system inhomogeneous of the system (Ref 35). CPE_{fl} represented the capacitance of the oxide film and the corrosion products; CPE_{dl} was the reaction capacitance of the double layer. The CPE was co-defined by two values, *Y* and *n*. C_{dl} was the reaction capacitance of Mg alloy matrix under the oxide film (Ref 33).

4.3 Discussion

In this study, aging treatment promoted the recrystallization and the dissolution of LPSO phase of Mg-Gd-Y-Zn-Zr alloy, which resulted in an improvement of corrosion resistance. The corrosion mechanisms of the as-extruded and peak-aged samples were discussed in the following.

In order to identify the potentials of the phases in the alloy, SKPFM was carried out for the as-extruded sample. The localized potential distribution and line-profile analysis of specimen combined with the morphology are shown in Fig. 6. The results indicated that the block-shaped LPSO exhibited a higher potential of about 1.65 V. However, when the line-profile contacted with the lamellar LPSO, the potential decreased sharply to about 1.5 V (Fig. 6b). As shown in Fig. 6(c), the granular RE-rich phase exhibited the highest potential of about 1.8 V, while the potential of matrix was about 1.6 V. It revealed that the potential values reduced as the following order: RE-rich phase > block-shaped LPSO > Mg matrix > lamellar LPSO phase. Therefore, it can be inferred

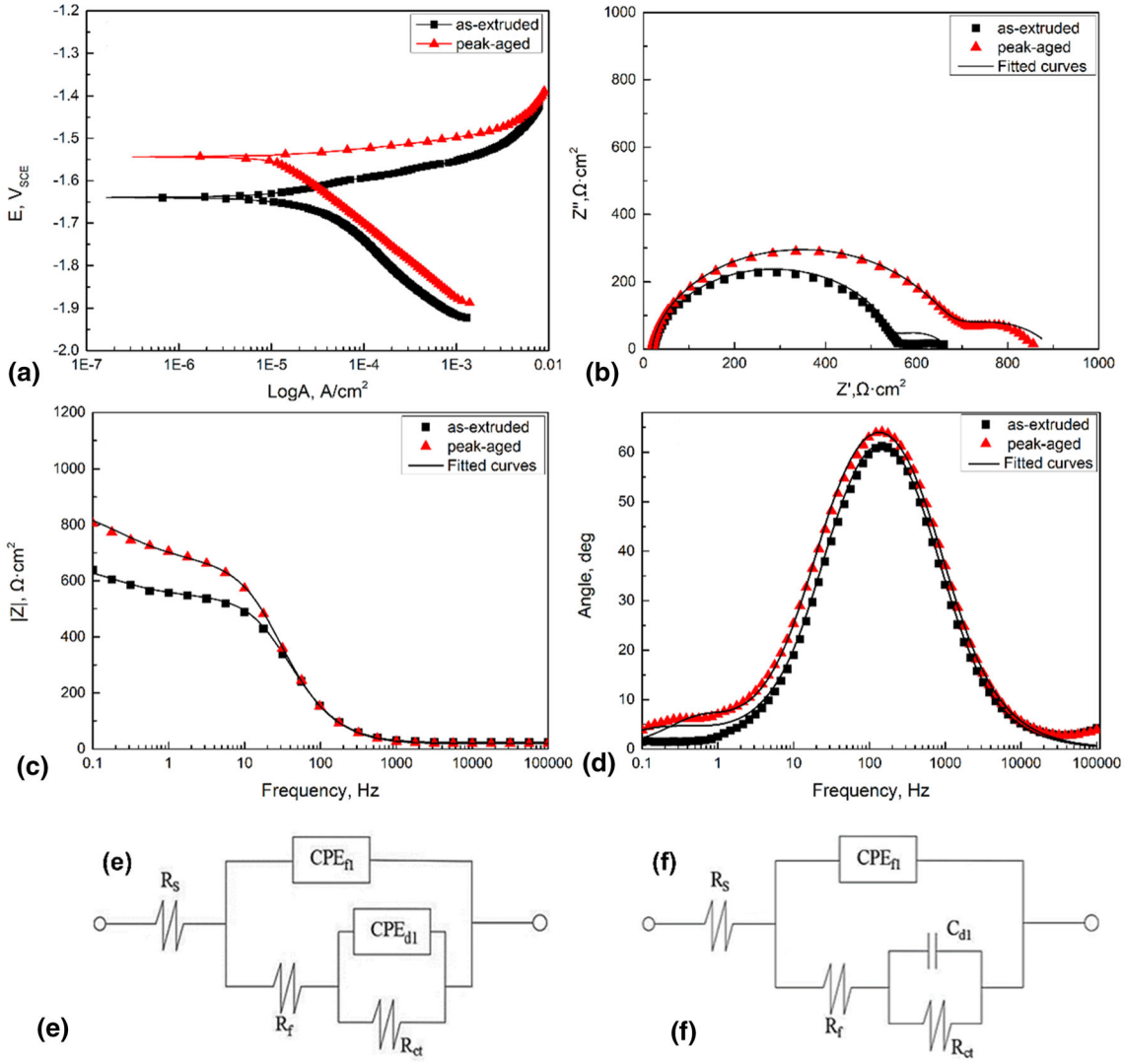

Fig. 5 Electrochemical measurement of the samples immersed in 3.5% NaCl solution: (a) polarization curves; (b) Nyquist plots; (c) and (d) corresponding Bode plots; equivalent circuit models for (e) the as-extruded and (f) peak-aged samples

Table 2 Fitting results of EIS and polarization curves measurement of Mg-Gd-Y-Zn-Zr-Ca in 3.5% NaCl solution

Samples	R_s, Ω cm^2	Y_{fl}, Ω^{-1} cm^{-2} s^n	n_{fl}	R_{ct}, Ω cm^2	Y_{dl}, Ω^{-1} cm^{-2} s^n	n_{d1}	C_{dl}	R_f, Ω cm^2	J_{corr}, A/cm^2	φ_{corr}, V
As-extruded	22.56	1.537×10^{-5}	0.9369	523.2	7.562×10^{-3}	0.773	…	120.2	2.029×10^{-5}	− 1.6395
peak-aged	22.90	1.60×10^{-5}	0.9265	694.1	…	…	2.462×10^{-3}	131.2	6.912×10^{-6}	− 1.5279

that the block-shaped LPSO phase and RE-rich phase with a higher potential than Mg matrix which would accelerate the dissolution of the matrix and lamellar LPSO phase. In addition, the potential difference implied that the lamellar LPSO phase was preferentially corroded because of micro-galvanic corrosion.

Figure 7 shows the corrosion morphologies of the as-extruded and peak-aged alloy after immersion for 2 and 24 h. More corrosion pits near the block-shaped area could be clearly observed in the as-extruded alloy (Fig. 7a) than the peak-aged alloy (Fig. 7b). From the magnified image in Fig. 7(a), it could be seen that the lamellar LPSO phase was more easily to be corroded compared with the recrystallized grains. When the immersion time was prolonged to 24 h, hollow structures could be detected in the as-extruded and peak-aged alloys. The remaining block-shaped LPSO phase and recrystallized grains streamlined along the extrusion direction. Deeper corrosion pits appeared in the as-extruded alloy (Fig. 7c) compared with the peak-aged sample (Fig. 7d). Additionally, a square shaped Mg_5(Gd, Y) phase was well preserved on the block-shaped LPSO phase (Fig. 7d), indicating that the block-shaped LPSO

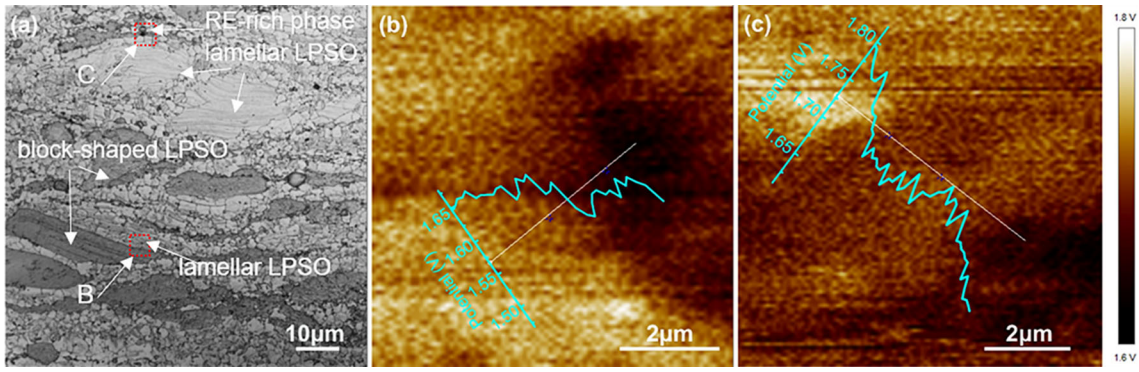

Fig.6 (a) Optical images and corresponding SKPFM results of (b) area B and (c) area C in a of the as-extruded alloy

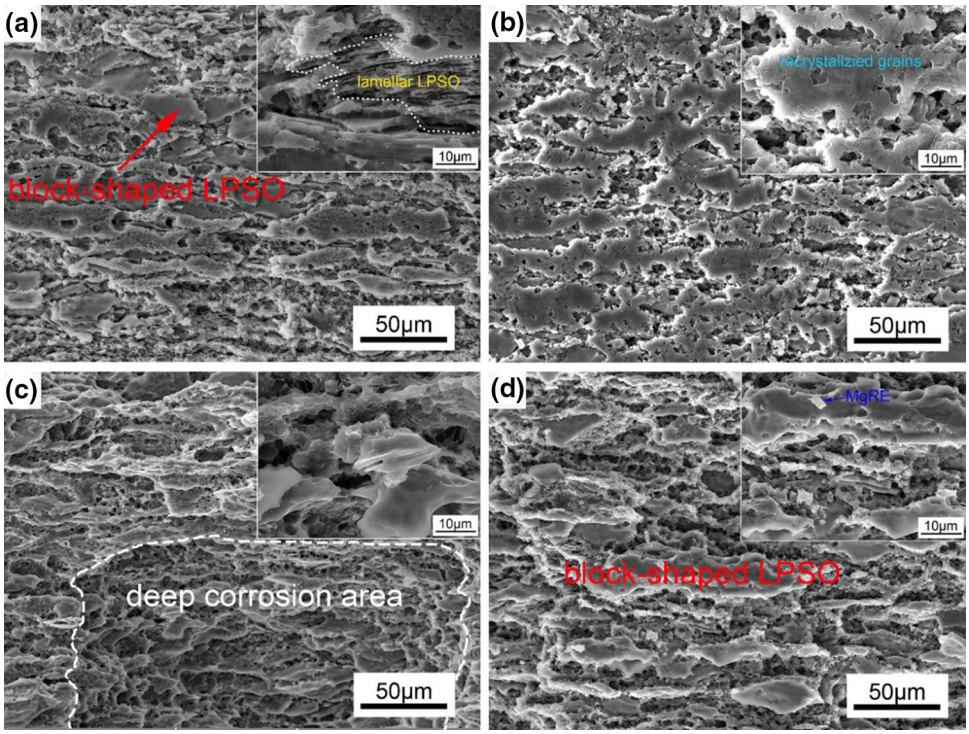

Fig. 7 Corrosion morphologies of the (a, c) as-extruded and (b, d) peak-aged samples immersion in 3.5% NaCl solution for (a, b) 2h and (c, d) 24 h

phase and the Mg_5(Gd, Y) phase had a better corrosion resistance compared with Mg matrix and the lamellar LPSO.

The cross section corrosion morphologies of the as-extruded and peak-aged alloy after immersion for 24 h are shown in Fig. 8. The corrosion depths for the as-extruded alloy and peak-aged alloy samples were about 302 μm (Fig. 8a) and 131 μm (Fig. 8c), respectively. Hence, it could be inferred that aging treatment was beneficial for the improvement of corrosion resistance. Additionally, the as-extruded alloy showed deep corrosion pits but the peak-aged alloy showed relatively shallow and uniform corrosion pits. Obvious micro-galvanic corrosion was observed in the vicinity of the block-shaped LPSO phase (Fig. 8b). This further confirmed that block-shaped LPSO phase was more stable compared with α-Mg and lamellar LPSO phase.

The schematic diagram of the corrosion process is shown in Fig. 9. At the initial stage of corrosion, the micro-galvanic among block-shaped LPSO, RE-rich phase, α-Mg matrix and the lamellar LPSO structure were formed. In this process, the lamellar LPSO phase at the surface of alloy with the lowest potential was corroded preferentially. Therefore, the as-extruded alloy corroded severely, and the corrosion pits even extended to the inside of the alloy along the lamellar LPSO, which showed a lager corrosion area and corrosion pits**.** However, since the reduction of the lamellar LPSO phase decreased the formation of micro-galvanic couples of the peak-aged sample (Ref 36), the peak-aged alloy exhibited shallow corrosion pits (Fig. 9e).

With corrosion proceeding, the corrosion extended into interior of the samples (Fig. 9c, f). The block-shaped LPSO phase with a higher potential acted as a micro-cathode (Ref 37), which accelerated the dissolution of the surrounding Mg matrix and lamellar LPSO phase until the dissolution or fall out of block-shaped LPSO (Figs. 8b, 9c). However, the volume of recrystallized grains was increased after aging treatment, accompanying the decrease of crystallographic defect (Ref

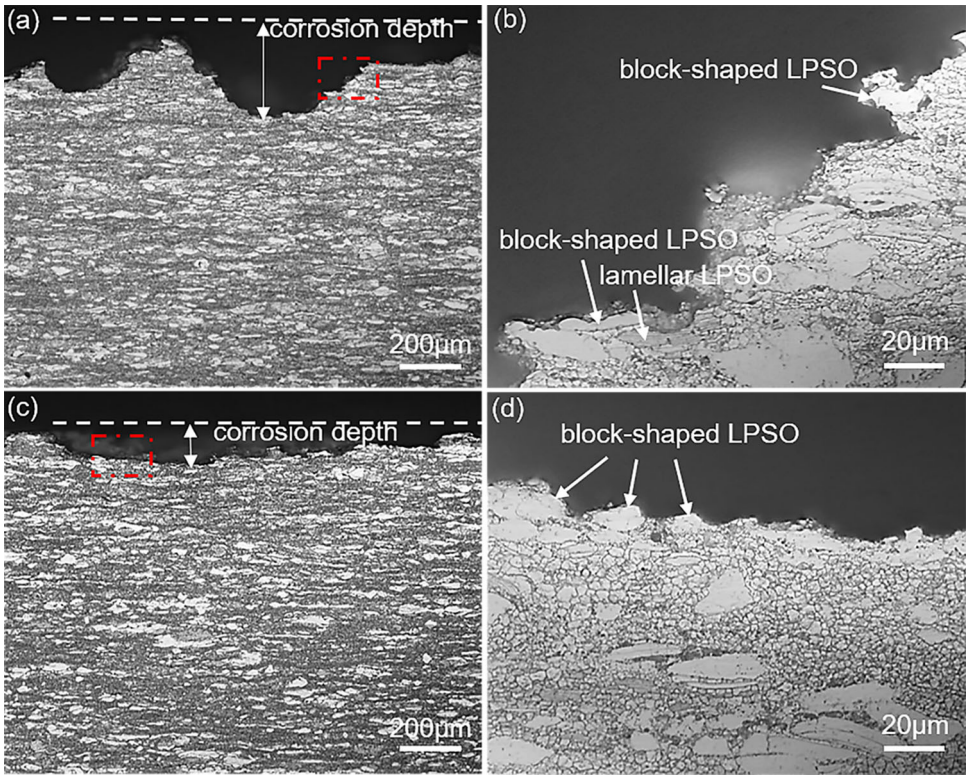

Fig. 8 The cross section morphology of the (a, b) as-extruded, (c, d) peak-aged sample after immersion in 3.5% NaCl solution for 24 h

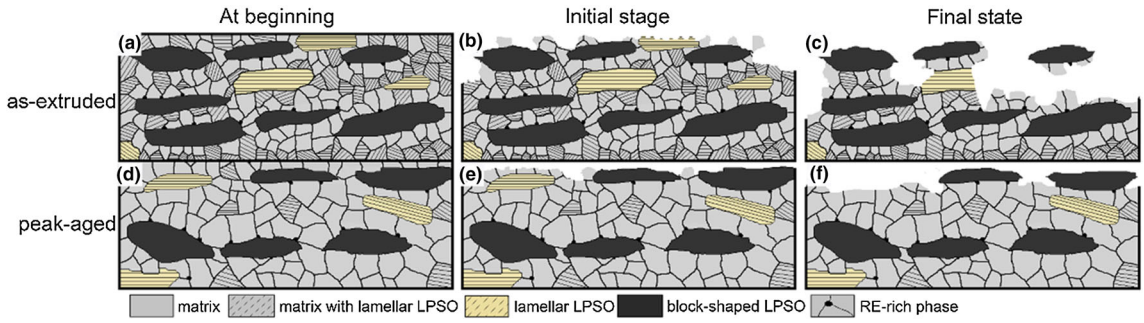

Fig. 9 Schematic diagram of corrosion development for (a-c) as-extruded, (d-f) peak-aged samples

38), which was easily corroded (Ref 39). The reduction of lamellar LPSO and the increase of recrystallized grains of the peak-aged alloy resulted in a better corrosion resistance (Fig. 9f).

4.4 Conclusions

The corrosion properties of the as-extruded and peak-aged Mg-8.9Gd-2.8Y-1.8Zn-0.4Zr-0.2Ca (wt.%) alloy were investigated in the present study. The main conclusions are summarized as follows:

1. The as-extruded and peak-aged Mg-8.99Gd-2.85Y-1.89Zn-0.42Zr-0.2Ca alloys are both composed of α-Mg, LPSO phase and Mg_5(Gd, Y) phase. However, part of LPSO phase was dissolved into the Mg matrix and recrystallization occurred during aging treatment.
2. Corrosion tests indicated that the potential values of the phase in the alloy reduced in the following order: RE-rich phase > block-shaped LPSO > Mg matrix > lamellar LPSO phase.
3. Aging treatment effectively improved the corrosion properties of the as-extruded Mg-Gd-Y-Zn-Zr alloy, which was mainly related to the homogeneous microstructure and the reduction of lamellar LPSO phase.

Acknowledgments

This work was supported by China Postdoctoral Science Foundation funded project (Nos. 2019M653703 and 2020T130523) and Shannxi Provincial Natural Science Foundation (No. 2018JQ8017).

References

1. K. Nie, X. Kang, K. Deng, Y. Guo, J. Han and Z. Zhu, Development of Mg-Zn-Y-Ca Alloys Containing Icosahedral Quasicrystal Phase Through Trace Addition of Y, *J. Mater. Res.*, 2018, **33**(18), p 2806–2816
2. S.H. Huang, Microstructure and Mechanical Properties of a Ag Micro-Alloyed Mg-5Sn Alloy, *J. Mater. Eng. Perform.*, 2018, **27**(7), p 3199–3205
3. H. Mirzadeh, High Strain Rate Superplasticity Via Friction Stir Processing (FSP): A Review, *Mater. Sci. Eng. A*, 2021, **819**, p 141499
4. A. Heinz, A. Haszler, C. Keidel, S. Moldenhauer, R. Benedictus and W.S. Miller, Recent Development in Aluminium Alloys for Aerospace Applications, *Mater. Sci. Eng. A*, 2000, **280**(1), p 102–107
5. H. Mirzadeh, Quantification of the Strengthening Effect of Rare Earth Elements During Hot Deformation of Mg-Gd-Y-Zr Magnesium Alloy, *J. Mater. Res. Technol.*, 2016, **5**(1), p 1–4
6. Y.Z. Du, D.J. Liu and Y.F. Ge, Effects of Ce Addition on Mechanical and Corrosion Properties of the As-Extruded Mg-Zn-Ca Alloy, *J. Mater. Eng. Perform.*, 2021, **30**(1), p 488–496
7. V.E. Bazhenov, S.S. Saidov, Y.V. Tselovalnik, O.O. Voropaeva, I.V. Plisetskaya, A.A. Tokar, A.I. Bazlov, V.A. Bautin, A.A. Komissarov, A.V. Koltygin and V.D. Belov, Comparison of Castability, Mechanical, and Corrosion Properties of Mg-Zn-Y-Zr Alloys Containing LPSO and W Phases, *Trans. Nonferr. Metal. Soc.*, 2021, **31**(5), p 1276–1290
8. M. Lotfpour, M. Emamy and C. Dehghanian, Influence of Cu Addition on the Microstructure, Mechanical, and Corrosion Properties of Extruded Mg-2%Zn Alloy, *J. Mate. Eng. Perform.*, 2020, **29**(5), p 2991–3003
9. L.B. Tong, J.H. Chu, W.T. Sun, C. Xu, D.N. Zou, K.S. Wang, S. Kamado and M.Y. Zheng, Achieving an Ultra-High Strength and Moderate Ductility in Mg-Gd-Y-Zn-Zr Alloy Via a Decreased-Temperature Multi-directional Forging, *Mater. Charact.*, 2021, **171**, p 110804
10. K. Li, V.S.Y. Injeti, R.D.K. Misra, L.G. Meng and X.G. Zhang, The Contribution of Long-Period Stacking-Ordered Structure (LPSO) to High Strength-High Ductility Combination and Nanoscale Deformation Behavior of Magnesium-Rare Earth Alloy, *Mater. Sci. Eng. A*, 2018, **713**, p 112–117
11. C.Q. Li, D.K. Xu, Z.R. Zeng, B.J. Wang, L.Y. Sheng, X.B. Chen and E.H. Han, Effect of Volume Fraction of LPSO Phases on Corrosion and Mechanical Properties of Mg-Zn-Y Alloys, *Mater. Des.*, 2017, **121**, p 430–441
12. J. Wang, T. Li, H.X. Li, Y.Z. Ma, K.N. Zhao, C.L. Yang, J.S. Zhang, Effect of Trace Ni Addition on Microstructure, Mechanical and Corrosion Properties of the Extruded Mg-Gd-Y-Zr-Ni Alloys for Dissoluble Fracturing Tools, *J. Magnes. Alloy.*, 2020 (**in press**)
13. S. Yin, W. Duan, W. Liu, L. Wu and Z. Zhang, Influence of Specific Second Phases on Corrosion Behaviors of Mg-Zn-Gd-Zr Alloys, *Corros. Sci.*, 2019, **166**, p 108419
14. M. Yamasaki, S. Izumi, Y. Kawamura and H. Habazaki, Corrosion and Passivation Behavior of Mg-Zn-Y-Al Alloys Prepared by Cooling Rate-Controlled Solidification, *Appl. Surf. Sci.*, 2011, **257**(19), p 8258–8267
15. Y. Wang, Y. Zhang, P. Wang, D. Zhang and H. Jiang, Effect of LPSO Phases and Aged-Precipitations on Corrosion Behavior of as-Forged Mg-6Gd-2Y-1Zn-0.3Zr Alloy, *J. Mater. Res. Technol.*, 2020, **9**(4), p 7087–7099
16. L. Wu and H. Li, Effect of Selective Oxidation on Corrosion Behavior of Mg-Gd-Y-Zn-Zr Alloy, *Corros. Sci.*, 2018, **142**, p 238–248
17. J.F. Nie and B.C. Muddle, Precipitation Hardening of Mg-Ca(-Zn) Alloys, *Scr. Mater.*, 1997, **37**(37), p 1475–1481
18. C. Xu, T. Nakata, X.G. Qiao, H.S. Jiang, W.T. Sun, Y.C. Chi, M.Y. Zheng and S. Kamado, Effect of Extrusion Parameters on Microstructure and Mechanical Properties of Mg-7.5Gd-2.5Y-3.5Zn-0.9Ca-0.4Zr (wt%) alloy, *Mater. Sci. Eng. A*, 2017, **685**, p 159–167
19. H. Jiang, X. Qiao, C. Xu, S. Kamado, K. Wu and M. Zheng, Influence of Size and Distribution of W Phase on Strength and Ductility of High Strength Mg-5.1Zn-3.2Y-0.4Zr-0.4Ca Alloy Processed by Indirect Extrusion, *J. Mater. Sci. Technol.*, 2018, **34**(2), p 277–283
20. T. Chen, Z. Chen, J. Shao, R. Wang, L. Mao and C. Liu, Evolution of LPSO Phases in a Mg-Zn-Y-Gd-Zr Alloy During Semi-Continuous Casting, Homogenization and Hot Extrusion, *Mater. Des.*, 2018, **152**, p 1–9
21. Y.M. Zhu, M. Weyland, A.J. Morton, K. Oh-Ishi, K. Hono and J.F. Nie, The Building Block of Long-Period Structures in Mg-RE-Zn Alloys—ScienceDirect, *Scr. Mater.*, 2009, **60**(11), p 980–983
22. C. Xu, S.W. Xu, M.Y. Zheng, K. Wu, E.D. Wang, S. Kamado, G.J. Wang and X.Y. Lv, Microstructures and Mechanical Properties of High-Strength Mg-Gd-Y-Zn-Zr Alloy Sheets Processed by Severe Hot Rolling, *J. Alloys Compd.*, 2012, **524**, p 46–52
23. H.X. Shao, Q.Z. Yang and L.X. Ma, Strengthening and Toughening Mechanisms in Mg-Zn-Y Alloy with a Long Period Stacking Ordered Structure, *Acta Mater.*, 2010, **58**(14), p 4760–4771
24. J.D. Robson, D.T. Henry and B. Davis, Particle Effects on Recrystallization in Magnesium–Manganese Alloys: Particle-Stimulated Nucleation, *Acta Mater.*, 2009, **57**(9), p 2739–2747
25. A. Jx, B. Zca, A. Js, C.A. Tao, L.A. Xia, A. Cl, Evolution of Long-Period Stacking Ordered Phases and Their Effect on Recrystallization in Extruded Mg-Gd-Y-Zn-Zr alloy During Annealing—ScienceDirect, *Mater. Charact.*, 2020, **167**. (**in press**)
26. Y.Z. Bao, Y. Adachi, Y. Toomine, P.G. Xu, T. Suzuki and Y. Tomota, Dynamic Recrystallization by Rapid Heating Followed by Compression for a 17Ni-0.2 C Martensite Steel, *Scr. Mater.*, 2005, **53**(12), p 1471–1476
27. L. Liu, X. Zhou, S. Yu, J. Zhang and Z. Su, Effects of Heat Treatment on Mechanical Properties of an Extruded Mg-4.3Gd-3.2Y-1.2Zn-0.5Zr Alloy and Establishment of its Hall–Petch Relation, *J. Magnes. Alloys*, 2020 (**in press**)
28. C. Xu, M.Y. Zheng, K. Wu, E.D. Wang and Y.T. Liu, Effect of Final Rolling Reduction on the Microstructure and Mechanical Properties of Mg-Gd-Y-Zn-Zr Alloy Sheets, *Mater. Sci. Eng. A*, 2013, **559**, p 232–240
29. C. Xu, M.Y. Zheng, K. Wu, E.D. Wang, G.H. Fan, S.W. Xu, S. Kamado, X.D. Liu, G.J. Wang and X.Y. Lv, Effect of Ageing Treatment on the Precipitation Behaviour of Mg-Gd-Y-Zn-Zr Alloy, *J. Alloys Compd.*, 2013, **550**, p 50–56
30. Y. Meng, J. Yu, K. Liu, H. Yu and H. Wang, The Evolution of Long-Period Stacking Ordered Phase and Its Effect on Dynamic Recrystallization in Mg-Gd-Y-Zn-Zr Alloy Processed by Repetitive Upsetting-Extrusion, *J. Alloys Compd.*, 2020, **828**, p 154454
31. J. Zhang, J. Xu, W. Cheng, C. Chen and J. Kang, Corrosion Behavior of Mg-Zn-Y Alloy with Long-Period Stacking Ordered Structures, *J. Mater. Sci. Technol.*, 2012, **28**(12), p 1157–1162
32. J. Liu, Y. Song, J. Chen, P. Chen, D. Shan and E.-H. Han, The Special Role of Anodic Second Phases in the Micro-galvanic Corrosion of EW75 Mg Alloy, *Electrochim. Acta*, 2016, **189**, p 190–195
33. F. Shi, C.-Q. Wang and Z.-M. Zhang, Microstructures, Corrosion and Mechanical Properties of As-Cast Mg-Zn-Y-(Gd) alloys, *Trans. Nonferr. Metal. Soc.*, 2015, **25**(7), p 2172–2180
34. J. Liu, L. Yang, C. Zhang, B. Zhang and T. Zhang, Significantly Improved Corrosion Resistance of Mg-15Gd-2Zn-0.39Zr Alloys: Effect of Heat-Treatment, *J. Mater. Sci. Technol.*, 2019, **35**(8), p 1644–1654
35. Y.S. Huang, X.T. Zeng, X.F. Hu and F.M. Liu, Corrosion Resistance Properties of Electroless Nickel Composite Coatings, *Electrochim. Acta*, 2004, **49**(25), p 4313–4319
36. Y. Wang, Y. Zhang, P. Wang, D. Zhang, B. Yu, Z. Xu and H. Jiang, Effect of LPSO Phases and Aged-Precipitations on Corrosion Behavior of as-Forged Mg-6Gd-2Y-1Zn-0.3Zr Alloy, *J. Mater. Res. Technol.*, 2020, **9**(4), p 7087–7099
37. X. Zhang, Q. Wang, F. Chen, Y. Wu, Z. Wang and Q. Wang, Relation Between LPSO Structure and Biocorrosion Behavior of Biodegradable GZ51K Alloy, *Mater. Lett.*, 2015, **138**, p 212–215
38. T. Zhang, Y. Shao, G. Meng, Z. Cui and F. Wang, Corrosion of Hot Extrusion AZ91 Magnesium Alloy: I-Relation Between the Microstructure and Corrosion Behavior, *Corros. Sci.*, 2011, **53**(5), p 1960–1968
39. G.L. Song and Z. Xu, The Surface, Microstructure and Corrosion of Magnesium Alloy AZ31 Sheet, *Electrochim. Acta*, 2010, **55**(13), p 4148–4161